# Poroelastic Effects on the Time- and Rate-Dependent Fracture of Polymer Gels

**Yalin Yu**
Department of Aerospace Engineering and Engineering Mechanics,
University of Texas,
Austin, TX 78712
e-mail: yalinyu19@gmail.com

**Nikolaos Bouklas**
Sibley School of Mechanical and Aerospace Engineering,
Cornell University,
Ithaca, NY 14853
e-mail: nb589@cornell.edu

**Chad M. Landis**
Department of Aerospace Engineering and Engineering Mechanics,
University of Texas,
Austin, TX 78712
e-mail: landis@utexas.edu

**Rui Huang**
Department of Aerospace Engineering and Engineering Mechanics,
University of Texas,
Austin, TX 78712
e-mail: ruihuang@mail.utexas.edu

*Fracture of polymer gels is often time- and rate-dependent. Subject to a constant load, a gel specimen may fracture immediately or after a delay (time-dependent, delayed fracture). When a crack grows in a gel, the fracture energy may depend on the crack speed (rate-dependent). The underlying mechanisms for the time- and rate-dependent fracture of gels could include local molecular processes, polymer viscoelasticity, and solvent diffusion coupled with deformation (poroelasticity). This paper focuses on the effects of poroelasticity. A path-independent, modified J-integral approach is adopted to define the crack-tip energy release rate as the energetic driving force for crack growth in gels, taking into account the energy dissipation by solvent diffusion. For a stationary crack, the energy release rate is time-dependent, with which delayed fracture can be predicted based on a Griffith-like fracture criterion. For steady-state crack growth in a long-strip specimen, the energy release rate is a function of the crack speed, with rate-dependent poroelastic toughening. With a poroelastic cohesive zone model, solvent diffusion within the cohesive zone leads to significantly enhanced poroelastic toughening as the crack speed increases, rendering a rate-dependent traction-separation relation. While most of the results are based on a linear poroelastic formulation, future studies may extend to nonlinear theories with large deformation. In addition to the poroelastic effects, other mechanisms such as viscoelasticity and local fracture processes should be studied to further understand the time and rate-dependent fracture of polymer gels.* [DOI: 10.1115/1.4045004]

*Keywords: polymer gels, J-integral, poroelasticity, delayed fracture, steady-state crack growth, flow and fracture, mechanical properties of materials*

## 1 Introduction

Polymer gels have been commonly used in biomedical applications [1–3]. Recently, polymer gels have been exploited as a class of soft active materials with potential applications in soft machines and soft robotics [4–7]. These applications have motivated the development of smart and tough gels [8–10]. However, it remains a challenge to accurately measure the fracture toughness of polymer gels [11], and a fundamental understanding of the fracture mechanisms in gels is still lacking [12]. Experimental measurements have reported a wide range of fracture toughness for polymer gels from ~1 J/m$^2$ for gelatin and agar gels [13,14] to ~$10^4$ J/m$^2$ for a tough gel with hybrid alginate–polyacrylamide networks [9]. As noted by Long and Hui [11], most of these measurements were interpreted by assuming that the gels were purely elastic. However, fracture is often time- and rate-dependent for polymer gels [15–18]. For example, in an experimental study on steady-state crack growth in gelatin gels, Baumberger et al. [18] found that the effective fracture energy was rate-dependent and increased with the crack speed (so-called "velocity toughening"). Recently, Tang et al. [17] conducted fracture experiments of polyacrylamide hydrogels under monotonic, static, and cyclic load; they observed time-dependent, delayed fracture below the critical load for fast fracture but above a threshold load.

To study delayed fracture of polymer gels, Wang and Hong [19] developed a nonlinear visco-poroelastic model with a pre-existing crack, and they found that the delay time depends on the size of a pre-existing crack in a similar way as diffusion-limited processes (a poroelastic effect). By assuming a specific size distribution of microcracks, they proposed a statistical theory on the lifetime prediction of a swollen gel. Bouklas et al. [20] studied the effects of solvent diffusion on the crack-tip fields and the energy release rate for stationary cracks in polymer gels using a nonlinear, transient finite element method. They proposed a modified *J*-integral for calculating the time-dependent crack-tip energy release rate for quasi-static crack growth in gels, with which delayed fracture was discussed as a possible scenario under certain chemo-mechanical conditions. For both analytical and numerical convenience, linear poroelasticity has also been used in studies concerning fractures of poroelastic materials. Atkinson and Craster [21] analyzed the fracture behavior in linearly poroelastic media under a prescribed internal pressure, and they obtained the stress intensity factor as a function of time using Laplace and Fourier transforms. Hui et al. [22] studied the short-time transient fields near the tip of a stationary crack in a linearly poroelastic solid. Yang and Lin [23] presented a numerical study on the time-dependent crack-tip fields in a linearly poroviscoelastic medium under constant applied stress. More recently, Yu et al. [24] presented an asymptotic analysis of the transient crack-tip fields for stationary cracks in polymer gels, with short-time and long-time limits for the stress intensity factor and the crack-tip energy release rate under different chemo-mechanical boundary conditions. Their numerical results suggested that the onset of crack growth may be delayed until the crack-tip energy release rate reaches a critical value.

To study steady-state crack growth in polymer gels, Noselli et al. [25] derived the energy release rate within the linearized, small-strain setting (linear poroelasticity) and predicted a poroelastic toughening effect as a result of solvent diffusion around the crack tip. In addition, they proposed a linear poroelastic cohesive zone model for the dependence of the effective toughness on crack speed. More recently, Yu et al. [26] considered steady-state crack growth in a long-strip specimen of finite width and found that the poroelastic toughening effect can lead to rate-dependent

Contributed by the Applied Mechanics Division of ASME for publication in the Journal of Applied Mechanics. Manuscript received August 22, 2019; final manuscript received September 23, 2019; published online September 30, 2019. Assoc. Editor: Yong-Wei Zhang.

  

fracture unless the crack speed is so high that the characteristic diffusion length scale is much smaller than the specimen size (small-scale diffusion). Both of these studies assumed plane strain conditions. However, thin specimens are commonly used in experiments, which can be modeled more accurately with plane stress conditions. The differences between the plain stress and plane strain conditions were examined in a recent work [27], where a nonlinear poroelastic cohesive zone model was proposed to further study the poroelastic effects on the rate-dependent fracture of polymer gels.

Based on the previous studies [20,24,26,27], we present in this paper the primary results concerning the poroelastic effects on the time- and rate-dependent fracture of polymer gels, including both delayed fracture and steady-state crack growth. In particular, the modified $J$-integral method is emphasized (Sec. 2) as an effective approach for calculating the crack-tip energy release rate as the energetic driving force for fracture in poroelastic gels, with which Griffith-like fracture criteria are proposed for delayed fracture with a stationary crack and for steady-state crack growth. While the method is generally applicable for linear and nonlinear poroelasticity, analytical and numerical results are presented here based on linear poroelasticity only, first for time-dependent (delayed) fracture in Sec. 3 and for rate-dependent, steady-state crack growth in Sec. 4. In the closing remarks (Sec. 5), we summarize the main findings to date and point out a few areas of potential interests for future studies.

## 2 $J$-Integral and Energy Release Rate

The classical $J$-integral [28] calculates the energy release within the contour as the crack grows straight ahead in the local crack-tip coordinates. If the material is purely elastic, the $J$-integral is path-independent and the energy release rate (per unit area of crack growth) provides a thermodynamic driving force for crack growth. However, if the material is inelastic and dissipates energy during deformation such as in metals (plasticity) and polymers (viscoelasticity), the energy release rate from the classical $J$-integral would also include the energy dissipated around the crack tip and within the contour, and consequently, it is no longer path-independent in general. In this case, the energetic driving force for crack growth may be determined by subtracting the energy dissipation (if possible) within the contour from the classical $J$-integral. Alternatively, if a cohesive zone is assumed at the crack tip, the $J$-integral with a contour around the cohesive zone without enclosing any other dissipative material can also be used to determine the driving force for crack growth [19,23]. In the case of polymer gels, energy dissipation may result from viscoelasticity [11,12], poroelasticity (solvent diffusion) [19,20,24–27], and background damage (due to network imperfection) [29], all of which may dissipate energy over a large volume around the crack, similar to ductile fracture in metals with large-scale yielding and energy dissipation by plasticity [30,31].

Despite extensive works on the fracture of viscoelastic materials in the 1970–1980s [32–37], the energetics of fracture with viscoelastic energy dissipation remains elusive, whereas the cohesive zone approach is commonly adopted. The mechanism of background damage due to network imperfection was recently proposed for polyacrylamide hydrogels [29], for which a detailed constitutive model with damage is not yet available for the calculation of energy dissipation. On the other hand, based on a nonlinear poroelastic theory of polymer gels with coupled elastic deformation and solvent diffusion, a modified $J$-integral was derived by Bouklas et al. [20] to calculate the energy release rate for crack growth in poroelastic gels, where the energy dissipation by solvent diffusion was subtracted from the classical contour integral. It was shown that the modified $J$-integral is path-independent for both transient and steady-state crack growth in poroelastic gels [24–27] without considering other energy dissipation mechanisms.

The modified $J$-integral for poroelastic gels can be written in two equivalent forms [20]:

$$J^* = \int_{\Gamma_0} \left( UN_1 - s_{\alpha J} N_J \frac{\partial x_\alpha}{\partial X_1} \right) d\Gamma - \int_{A_0} \mu \frac{\partial C}{\partial X_1} dA \tag{1}$$

or

$$J^* = \int_{\Gamma_0} \left( \hat{U}N_1 - s_{\alpha J} N_J \frac{\partial x_\alpha}{\partial X_1} \right) d\Gamma + \int_{A_0} C \frac{\partial \mu}{\partial X_1} dA \tag{2}$$

where $U = U(\boldsymbol{F}, C)$ is the free energy density function in terms of the deformation gradient $\boldsymbol{F}$ and the solvent concentration $C$, and $\hat{U} = U - \mu C$ is Legendre transform of the free energy density function that yields a function of the deformation gradient $\boldsymbol{F}$ and the chemical potential of the solvent $\mu$. Here, the contour $\Gamma_0$ is drawn in a homogeneous reference configuration with $N_J$ being the outward unit normal vector, and $A_0$ being the enclosed area (see Fig. 1); $s_{\alpha J}$ is the first Piola-Kirchhoff stress, $x_\alpha$ is the location coordinate of the material point in the current (deformed) configuration, and $X_J$ is the location coordinate in the reference configuration; the crack is assumed to lie in the $X_1 - X_3$ plane with a crack front perpendicular to the $X_1 - X_2$ plane in the reference configuration.

The second form of the modified $J$-integral in Eq. (2) is preferable for numerical calculations by the finite element method [20], because it does not require the calculation of the derivatives of the solvent concentration, which would require higher-order interpolations of the concentration field [38]. A domain integral method was developed along with a nonlinear transient finite element method to calculate the modified $J$-integral [20]. We note that similar forms of modified $J$-integrals were developed previously for the hygro-thermo-elastic fracture [39,40] and for the fracture of battery electrodes with solute diffusion [41].

The nonlinear poroelastic theory for large deformation and solvent diffusion in polymer gels can be linearized for infinitesimal deformation near a homogeneously swollen state to yield a linear poroelastic formulation [42], taking the same form as Biot's theory of linear poroelasticity [43]. With the linear poroelastic formulation, the modified $J$-integral is also linearized to yield [26]:

$$J^* = \int_{\Gamma_0} \left( \hat{\phi} n_1 - \sigma_{ij} n_j \frac{\partial u_i}{\partial x_1} \right) d\Gamma + \int_{A_0} (c - c_0) \frac{\partial \mu}{\partial x_1} dA \tag{3}$$

where the linearized free energy density function is

$$\hat{\phi} = G\left[ \varepsilon_{ij}\varepsilon_{ij} + \frac{\nu}{1-2\nu} (\varepsilon_{kk})^2 \right] - (\mu - \mu_0)(c - c_0) \tag{4}$$

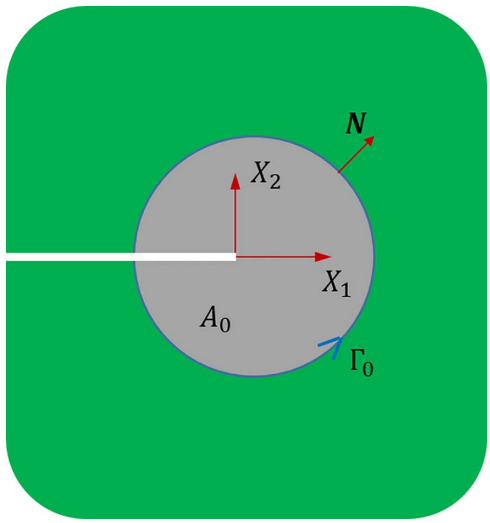


**Fig. 1 A crack in a reference configuration with a contour around the crack tip for $J$-integral**

Here, $\sigma_{ij}$ is the Cauchy stress, $\varepsilon_{ij}$ is the linear strain, $u_i$ is the displacement, $c$ is the solvent concentration, $G$ is the shear modulus, and $\nu$ is the Poisson's ratio (drained), all defined with respect to a homogeneous initial state of the gel with an initial solvent concentration $c_0$ and correspondingly, an initial chemical potential of the solvent $\mu_0$; the contour $\Gamma_0$ is drawn in the initial configuration as well. While the nonlinear form of the modified $J$-integral in Eq. (1) or (2) gives the energy release rate per unit area in the reference configuration (typically, the un-swollen dry state), the linear form in Eq. (3) is set up in the initial swollen state and thus gives the energy release rate per unit area in this initial state; the two differ by a factor of $\lambda_0^2$, with $\lambda_0$ being the linear swelling ratio of the gel relative to the dry state of the polymer network.

With the modified $J$-integral as the crack-tip energy release rate, a Griffith-like fracture criterion may be proposed for a stationary crack and for steady-state crack growth in poroelastic gels. In the case of a stationary crack, the modified $J$-integral is time-dependent [20,24] and the onset of crack growth may be predicted when the modified $J$-integral reaches a critical value, namely

$$J^*(t) = \Gamma_{c0} \tag{5}$$

where $\Gamma_{c0}$ is the fracture energy for initiation of crack growth and may depend on the polymer network structure as well as the solvent content of the gel. For steady-state crack growth, the modified $J$-integral is rate-dependent (a function of crack speed $\dot{a}$) [25–27], which must be equal to the rate-dependent fracture energy at the same crack speed, namely,

$$J^*(\dot{a}) = \Gamma_{SS}(\dot{a}) \tag{6}$$

where $\Gamma_{SS}(\dot{a})$ is the steady-state fracture energy and may depend on the fracture processes at the crack tip. The specific fracture processes may be time- and rate-dependent in general. Following the spirit of small-scale yielding, we assume a small-scale fracture process zone so that the detailed fracture processes are not explicitly considered, but the rate-dependent fracture energy may still be determined by calculating the modified $J$-integral on the left-hand side of Eq. (6) along with the measurement of the crack speed.

The modified $J$-integral on the left-hand side of Eqs. (5) and (6) differs from the classical $J$-integral in that the energy dissipation by solvent diffusion within the contour has been subtracted because this dissipated energy cannot be released upon crack growth, namely

$$J^* = J - J_d \tag{7}$$

where $J$ is the classical $J$-integral and $J_d$ is the energy dissipation rate within the contour. For poroelastic gels, both $J$ and $J_d$ are path-dependent, but $J^*$ is path-independent [20]. By the second law of thermodynamics, $J_d \geq 0$ in all cases. With a remote contour along the boundary of a fracture specimen, the classical $J$-integral required to initiate the growth of a stationary crack is then

$$J_c = \Gamma_{c0} + J_d \tag{8}$$

which is greater than the intrinsic fracture energy $\Gamma_{c0}$. Similarly, for steady-state crack growth, the classical $J$-integral with a remote contour is

$$J_{ss}(\dot{a}) = \Gamma_{ss}(\dot{a}) + J_d(\dot{a}) \tag{9}$$

which is greater than the intrinsic steady-state fracture energy $\Gamma_{ss}(\dot{a})$. Therefore, the apparent fracture energy by the classical $J$-integral is generally greater than the intrinsic fracture energy, and the difference is due to the energy dissipation associated with solvent diffusion in the gel, namely, poroelastic toughening [25]. Furthermore, it is noted that the amount of poroelastic toughening may depend on the specimen size and geometry unless solvent diffusion is confined within a small region (compared to the specimen size) around the crack tip.

## 3 Time-Dependent (Delayed) Fracture

A stationary center-crack model was studied in detail previously [20,24], which is summarized here as an example. Consider a specimen with a stationary center crack (Fig. 2), subject to uniaxial tension by either displacement or load (traction) controlled step loading under plane strain conditions. The initial state of the gel is assumed to be stress free and homogeneously swollen, with a solvent concentration $c_0$ corresponding to the chemical potential $\mu_0 = 0$. The specimen may be immersed in an external solution so that all of the boundaries (including the crack faces) are in contact with the external solution where the chemical potential $\mu = 0$ is assumed. Alternatively, if the specimen is not immersed, we assume that all of the boundaries are impermeable to solvent diffusion. For simplicity, only the results from the linear poroelastic analysis [24] are discussed here, whereas the nonlinear results [20] are qualitatively similar.

Instantaneously upon a step loading ($t = 0^+$), if the poroelastic material behaves like an incompressible, linearly elastic material with $\nu = 0.5$ (undrained), the energy release rate would be

$$J_0 = \frac{K_{I0}^2}{4G} \tag{10}$$

where $K_{I0}$ is the instantaneous stress intensity factor. For an infinitely large specimen ($h/a \to \infty$), $K_{I0} = 4G\varepsilon_h\sqrt{\pi a}$ under displacement control with $\varepsilon_h$ being the applied remote strain, or $K_{I0} = \sigma_h\sqrt{\pi a}$ under load control with $\sigma_h$ being the applied remote stress, where $a$ is the half crack length and $h$ is the half-width of the specimen.

The instantaneous elastic deformation around the crack tip leads to an inhomogeneous field of the chemical potential, which drives solvent diffusion in the poroelastic specimen. Even at infinitesimal time increments ($t \to 0^+$), there exists a diffusion zone around the crack tip, which may influence the stress intensity factor and the energy release rate [24]. By dimensional considerations, the energy release rate can be written as

$$\frac{J^*}{J_0} = \Lambda\left(\frac{t}{\tau}, \frac{h}{a}, \nu\right) \tag{11}$$

where $\tau = a^2/D^*$ is the characteristic diffusion time with an effective diffusivity $D^*$, $\nu$ is Poisson's ratio (drained), and the dimensionless function on the right-hand side is to be determined numerically and depends on the chemo-mechanical conditions (displacement or load control, immersed or not immersed) [24]. For linearly

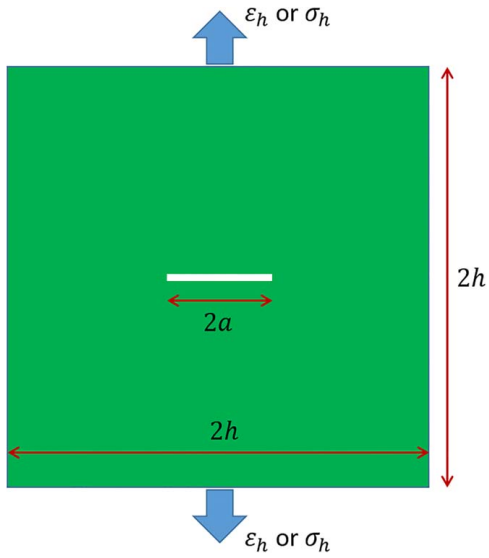


**Fig. 2 Schematic of a stationary center-crack model**

**Table 1 Short-time and long-time limits of the crack-tip energy release rate for the linearly poroelastic center-crack model**

| | | Short-time limit | Long-time limit |
|---|---|---|---|
| Immersed | Displacement control | $J^*(t \to 0^+) = J_0\left[\frac{1}{2(1-\nu)}\right]^{0.47}$ | $J^*(t \to \infty) = \frac{J_0}{2(1-\nu)}$ |
| | Load control | | $J^*(t \to \infty) = 2(1-\nu)J_0$ |
| Not-immersed | Displacement control | $J^*(t \to 0^+) = J_0$ | $J^*(t \to \infty) = 1.496J_0$[a] |
| | Load control | | $J^*(t \to \infty) = 2(1-\nu)J_0$ |

[a]Based on numerical results for $h/a = 10$ and $\nu = 0.24$ [24].

poroelastic materials, analytical limits for the energy release rate can be found at the short-time and long-time limits as listed in Table 1.

**3.1 Short-Time Limits.** At the short-time limit ($0 < t/\tau \ll 1$), the stress intensity factor is found to be [21,24]

$$K_I(t \to 0^+) = K_{I0}\left[\frac{1}{2(1-\nu)}\right]^{\alpha} \tag{12}$$

where $\alpha \approx 0.735$ for the immersed case and $\alpha = 0.5$ for the not-immersed case. Therefore, in both the immersed and not-immersed cases, $K_I(t \to 0^+) < K_{I0}$ as long as $\nu < 0.5$.

Correspondingly, the energy release rate at the short-time limit is obtained for the immersed and not-immersed cases as [24]

$$J^*(t \to 0^+) = J_0\left[\frac{1}{2(1-\nu)}\right]^{2\alpha-1} \tag{13}$$

Thus, for the immersed case ($\alpha \approx 0.735$), $J^*(t \to 0^+) < J_0$; and for the not-immersed case ($\alpha = 0.5$), $J^*(t \to 0^+) = J_0$.

**3.2 Long-Time Limits.** At the long-time limit ($t \to \infty$), the chemical potential becomes homogenous so that the specimen reaches both chemical and mechanical equilibrium (assuming no crack growth) and the linear poroelasticity problem becomes identical to a linear elasticity problem. For the immersed case, the stress intensity factor at the long-time limit is exactly the same as the elastic case with the (drained) Poisson's ratio ($\nu$). Under displacement control, we obtain [24]

$$K_I(t \to \infty) = \frac{K_{I0}}{2(1-\nu)} \tag{14}$$

which is smaller than the short-time limit given by Eq. (12) with $\nu < 0.5$. Under load control, the elastic stress intensity factor is independent of Poisson's ratio. As a result, the stress intensity factor at the long-time limit is simply:

$$K_I(t \to \infty) = K_{I0} \tag{15}$$

which is greater than the short-time limit in Eq. (12) for the immersed case [24].

Correspondingly, the energy release rate at the long-time limit for the immersed case is [24]

$$J^*(t \to \infty) = \frac{J_0}{2(1-\nu)} \tag{16}$$

under displacement control and

$$J^*(t \to \infty) = 2(1-\nu)J_0 \tag{17}$$

under load control. Therefore, the energy release rate as a function of time depends on the loading conditions, with different long-time limits for displacement and load control.

For the not-immersed case, under load control, the long-time limit of the stress intensity factor is the same as Eq. (15). Under displacement control, the long-time limit is also the same if $h/a \gg 1$, but slightly different for a finite specimen [24]: $K_I(t \to \infty) = 0.993K_{I0}$ for $h/a = 10$ and $\nu = 0.24$.[1] Similarly, the energy release rate at the long-time limit for $h/a \gg 1$ is the same as Eq. (17) for the not-immersed cases, but slightly different for a finite specimen under displacement control: $J^*(t \to \infty) = 1.496J_0$ for $h/a = 10$ and $\nu = 0.24$.

**3.3 Numerical Results.** Based on the linear poroelastic formulation, a finite element method was developed to solve the associated initial/boundary value problems [24]. By the modified $J$-integral, we calculated the crack-tip energy release rate ($J^*$) in the linearly poroelastic center-crack model (Fig. 2), which confirmed the predictions for the short-time and long-time limits in Table 1. Figure 3(*a*) shows the normalized energy release rate as a function of the normalized time for both the immersed and not-immersed specimens under displacement-controlled step loading. For the not-immersed case, the normalized energy release rate increases monotonically over time, from the short-time limit to the long-time limit. For the immersed case, however, the normalized energy release rate first increases and then decreases, approaching a long-time limit that is smaller than the short-time limit. The non-monotonic evolution is a result of solvent diffusion from both the crack faces and the outer boundaries of the specimen as discussed in Ref. [20]. Figure 3(*b*) shows the normalized energy release rates under load control. For the not-immersed case, the behavior is similar to that under displacement control in Fig. 3(*a*), except for a slightly different long-time limit due to a finite specimen size ($h/a = 10$). On the other hand, the behavior for the immersed case is different from that in Fig. 3(*a*). While the short-time limit is the same for both displacement and load control, the long-time limits are different for the immersed case. In contrast to the non-monotonic variation under displacement control (Fig. 3(*a*)), the energy release rate increases monotonically under load control, approaching the same long-time limit as for the not-immersed case. Thus, under different loading conditions, the fracture behavior could be different for the immersed specimens.

**3.4 Delayed Fracture.** By the fracture criterion in Eq. (5), a stationary crack in a poroelastic gel would start growing once the time-dependent energy release rate ($J^*$) reaches a critical value ($\Gamma_{c0}$). Depending on the applied load (either displacement or load control) as well as the chemical boundary condition (immersed or not-immersed), the crack may grow immediately or after a time delay or may not grow at all. According to the numerical results in Fig. 3, except for the immersed case under displacement-controlled loading, the energy release rate ($J^*$) increases monotonically over time. In these cases, the crack would grow immediately if the short-time limit of the energy release rate is greater than the

[1]In the present work, $\nu$ is the drained Poisson's ratio in linear poroelasticity as defined in Ref. [42] unless noted otherwise. The undrained Poisson's ratio is taken to be 0.5 assuming incompressibility for both the polymer and the solvent. The difference between the drained and undrained Poisson's ratios depends on the initial solvent concentration in the gel. The value $\nu = 0.24$ is used in numerical simulations for a typical polymer gel with an initial solvent concentration $\Omega c_0 = 0.97$ (equivalent to a solvent volume fraction of 97%).

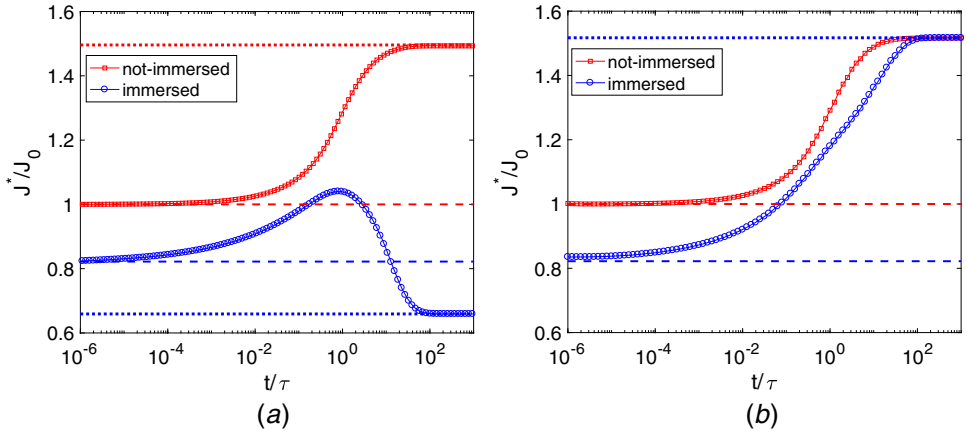


**Fig. 3 Normalized energy release rate ($J^*/J_0$) versus the normalized time ($t/\tau$) for the immersed and not-immersed center-crack models with $h/a = 10$ and $\nu = 0.24$. (*a*) under displacement control and (*b*) under load control. The horizontal dashed and dotted lines are the short-time and long-time limits, respectively.**

fracture toughness, i.e., $J^*(t \to 0^+) > \Gamma_{c0}$, but would never grow if the long-time limit is lower than the fracture toughness, i.e., $J^*(t \to \infty) < \Gamma_{c0}$; in between, delayed crack growth is predicted if $J^*(t \to 0^+) < \Gamma_{c0} < J^*(t \to \infty)$. Taking $J_0$ as the applied loading parameter (corresponding to the classical $J$-integral with a remote contour), the delay time may be predicted by Eq. (5) as shown in Fig. 4. For the center-crack model with $h/a = 10$ and $\nu = 0.24$, the crack would never grow if $J_0 < 0.66\Gamma_{c0}$ (a threshold for delayed fracture), immersed or not. For the not-immersed case, the crack grows immediately if $J_0 > \Gamma_{c0}$, whereas delayed fracture would occur if $0.66\Gamma_{c0} < J_0 < \Gamma_{c0}$ (subcritical), with the delay time decreasing as the applied load ($J_0$) increases. For the immersed case, the crack grows immediately only if $J_0 > 1.22\Gamma_{c0}$ (supercritical), with 22% toughening due to the poroelastic effect. Hence, the gel would appear to be tougher when immersed. Furthermore, under the same normalized loading when $0.66\Gamma_{c0} < J_0 < \Gamma_{c0}$, Fig. 4 predicts that the delay time would be longer for the immersed case than not-immersed.

Experimentally, delayed fracture has been observed in polymer gels [15–17] as well as many other materials [32,44–48]. For polymer gels, the delayed fracture may result from thermally activated crack nucleation [15], stress-enhanced bond rupture and dissociation [16], viscoelasticity (creep), and poroelasticity (solvent diffusion) [19–24]. Recently, Tang et al. [17] observed delayed fracture of polyacrylamide hydrogels when the applied energy release rate ($J_0$) was below the critical load for fast fracture and above a threshold value, while the delay time increased as the applied energy release rate decreased. This observation is qualitatively consistent with Fig. 4, where the critical energy release rate for fast fracture is set by the short-time limit and the threshold for delayed fracture is set by the long-time limit. In between, the delay time for the onset of crack growth decreases sharply with increasing load ($J_0$) and can be written as

$$t_b = \frac{a^2}{D^*} \cdot f\left(\frac{J_0}{\Gamma_{c0}}, \frac{h}{a}, \nu\right) \tag{18}$$

where the dimensionless function $f(\ldots)$ depends on the normalized load ($J_0/\Gamma_{c0}$) as well as the specimen geometry and the chemo-mechanical boundary conditions.

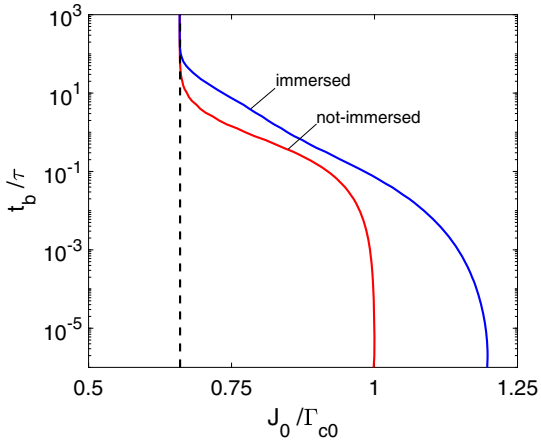


**Fig. 4 Normalized delay time ($t_b/\tau$) for the onset of crack growth for the linearly poroelastic center-crack model under load control**

## 4 Rate-Dependent Fracture: Steady-State Crack Growth

For steady-state crack growth in polymer gels, an infinitely long-strip specimen with a semi-infinite crack was considered, first under plane strain conditions [26] and then under plane stress conditions [27]; both were based on the linear poroelastic formulation for polymer gels. Theoretically, there are subtle differences between the plane stress and plane strain conditions, such as the effective diffusivity and the asymptotic crack-tip fields for the solvent concentration and chemical potential [27]. Experimentally, thin-sheet specimens are commonly used such as the pure shear tests, which are close to the plane stress conditions. As shown in Fig. 5, the strip width is $2h$, with a semi-infinite crack lying in the mid-plane. Subjected to an opening displacement $\pm\Delta$ applied to the upper and lower edges of the strip, the crack grows and reaches a steady-state with a constant crack speed $\dot{a}$. Similar specimens have been used in experiments for various materials including rubber [49] and gels [11,18].

With respect to the moving coordinate (for an observer traveling with the crack tip), the mechanical equilibrium equation remains

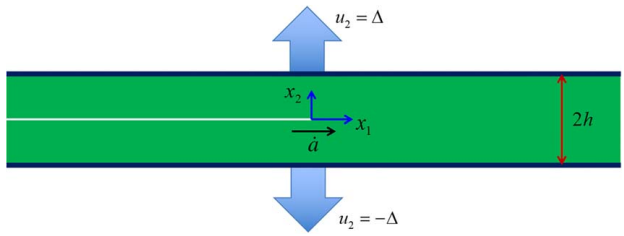


**Fig. 5 Schematic of a long-strip specimen with steady-state crack growth in the $x_1$ direction**

unchanged, while the equation for solvent diffusion becomes time-*independent* but instead depends on the steady-state crack speed ($\dot{a}$). The steady-state crack model (Fig. 5) has two relevant length scales: the specimen half-width $h$ and the steady-state diffusion length $l_{ss} = D^*/\dot{a}$ [26,27]. The ratio between the two length scales defines a dimensionless number

$$\text{Pe} = \frac{h}{l_{ss}} = \frac{\dot{a}h}{D^*} \tag{19}$$

which is called the Péclet number for advection-diffusion problems [50]. Note that the Péclet number is slightly different under plane stress and plane strain conditions due to the difference in the effective diffusivity [27].

If the specimen is made of a material that is linearly elastic and incompressible, the energy release rate for steady-state crack growth in the pure shear test is simply:

$$J_e = 4G\varepsilon_\infty^2 h \tag{20}$$

where $\varepsilon_\infty = \Delta/h$. For a linearly poroelastic long-strip specimen, the normalized energy release rate ($J^*/J_e$) for the steady-state crack growth depends on two dimensionless parameters: the Péclet number ($\text{Pe} = h/l_{ss}$) and the (drained) Poisson's ratio ($\nu$), namely

$$\frac{J^*}{J_e} = \Lambda_{ss}(\text{Pe}, \nu) \tag{21}$$

A stabilized finite element method was developed for the steady-state crack growth model [26,27]. A subtle difference between the plane strain and plane stress is the boundary condition along the upper and lower edges ($x_2 = \pm h$) of the specimen: while a constant displacement $u_2 = \pm h\varepsilon_\infty$ is applied for both cases, the displacement $u_1 = 0$ is assumed in the plane stress model [27], but the traction $\sigma_{21} = 0$ is assumed in the plane strain model [26] so that a uniform stretch in the $x_2$ direction far ahead of the crack tip is possible with the incompressible deformation under the plane strain conditions.

**4.1 Slow Crack Limit ($\text{Pe} \ll 1$).** For the slow crack limit, the solvent diffusion is primarily one-dimensional (1D) in the $x_1$ direction ahead of the crack tip ($x_1 > 0$), which can be modeled approximately by a 1D model for both plane stress and plane strain conditions [26,27]. It was found that, at the slow crack limit, both the chemical potential and opening stress ahead of the crack tip (for $x_1 > h$) vary exponentially with a characteristic diffusion length scale $l_{ss} \gg h$. Correspondingly, the energy release rate can be calculated by the modified $J$-integral for the slow crack limit as

$$J^*(\text{Pe} \ll 1) = \frac{J_e}{2(1-\nu)} \tag{22}$$

which is the same for both immersed and not-immersed cases [26,27].

**4.2 Fast Crack Limit ($\text{Pe} \gg 1$).** At the fast crack limit, $l_{ss} \ll h$ so that solvent diffusion is largely confined to a small region around the crack tip (small-scale diffusion). In this case, a crack-tip model may be constructed [25–27], where the asymptotic elastic crack-tip solution can be imposed as the remote boundary condition. We note that such a crack-tip model is strictly possible for the immersed case only, when there exists an elastic crack-tip solution [26]. Nevertheless, the numerical results suggested that the energy release rate approaches the same fast crack limit for both the immersed and not-immersed cases [26,27]. On the other hand, different fast crack limits were obtained under plane stress and plane strain conditions. As listed in Table 2, the energy release rate for the fast crack limit under the plane strain conditions is identical to the slow crack limit in Eq. (22), whereas the fast crack limit under the plane stress conditions is higher (for $0 \le \nu < 0.5$) [27]:

$$J^*(\text{Pe} \gg 1) = \frac{2}{3}(1+\nu)J_e \tag{23}$$

**Table 2 Slow-crack and fast-crack limits of the energy release rate for steady-state crack growth in linearly poroelastic specimens**

| | Slow-crack limit | Fast-crack limit |
|---|---|---|
| Plane strain | $J^*(\text{Pe} \ll 1 \text{ or } \text{Pe} \gg 1) = \frac{J_e}{2(1-\nu)}$ | |
| Plane stress | $J^*(\text{Pe} \ll 1) = \frac{J_e}{2(1-\nu)}$ | $J^*(\text{Pe} \gg 1) = \frac{2}{3}(1+\nu)J_e$ |

Both limits in Eqs. (22) and (23) become the same as the elastic value in Eq. (20) when $\nu = 0.5$, which implies no solvent diffusion and hence the material is purely elastic (and incompressible). When $0 \le \nu < 0.5$, $J^* < J_e$ at both limits due to poroelastic effects. In other words, the energy release rate at the crack tip is smaller than the classical $J$-integral applied at the remote boundary because part of the supplied energy has been dissipated by solvent diffusion in the poroelastic specimen. The poroelastic effect thus solely depends on the (drained) Poisson's ratio at the two limits. For polymer gels, the (drained) Poisson's ratio depends on the initial solvent concentration and the solvent-polymer interaction [42].

**4.3 Numerical Results.** Figure 6 shows the numerical results for the normalized energy release rate as a function of the normalized crack speed (Pe) for both the immersed and not-immersed cases. Under the plane strain conditions (Fig. 6(*a*)), the normalized energy release rate depends on the normalized crack speed non-monotonically, with a peak at $\text{Pe} \sim 10$ for the immersed case and at $\text{Pe} \sim 3$ for the not-immersed case. While the slow crack and fast crack limits are the same for both the immersed and not-immersed cases, the peak is higher for the immersed case. In contrast, under the plane stress conditions (Fig. 6(*b*)), the normalized energy release rate depends on the normalized crack speed monotonically, except for a shallow peak at $\text{Pe} \sim 100$ for the immersed case.[2] In particular, the normalized energy release rate is considerably higher under the plane stress condition at the fast crack limit, indicating lower energy dissipation by solvent diffusion. This difference between plane strain and plane stress conditions may be understood as a result of different hydrostatic stress components that relate directly to the chemical potential and hence the solvent diffusion. The hydrostatic stress is higher under the plane strain conditions, thus leading to higher energy dissipation by solvent diffusion. This is opposite to the effect of plasticity, where energy dissipation is associated with the deviatoric (shear) stress and thus is relatively lower under the plane strain conditions [51].

**4.4 Rate-Dependent Fracture.** By the fracture criterion in Eq. (6), when the crack grows in a steady-state, the crack-tip energy release rate ($J^*$) must be equal to the intrinsic steady-state fracture toughness ($\Gamma_{ss}$) of the gel. Thus, the fracture toughness as a function of crack speed can be determined by measuring the steady-state crack speed ($\dot{a}$) in a long-strip specimen as a function of the applied strain ($\varepsilon_\infty = \Delta/h$), namely

$$\Gamma_{ss}(\dot{a}) = J^* = 4G\varepsilon_\infty^2 h \cdot \Lambda_{ss}\left(\frac{\dot{a}h}{D^*}, \nu\right) \tag{24}$$

where the dimensionless function $\Lambda_{ss}\left(\frac{\dot{a}h}{D^*}, \nu\right)$ can be calculated as shown in Fig. 6 for either plane stress or plane strain conditions. The poroelastic properties ($G$, $\nu$, and $D^*$) of the gel must be determined separately by independent measurements. On the other hand, the classical $J$-integral ($J_e = 4G\varepsilon_\infty^2 h$) is often taken as the

[2]Under plane stress conditions, the surfaces of the thin specimen are assumed to be impermeable to solvent diffusion for both the immersed and non-immersed cases so that no solvent diffusion occurs in the out-of-plane direction. Otherwise, in the immersed case, the chemical potential would be nearly a constant in equilibrium with the external solution and the problem become purely elastic (rate-independent).

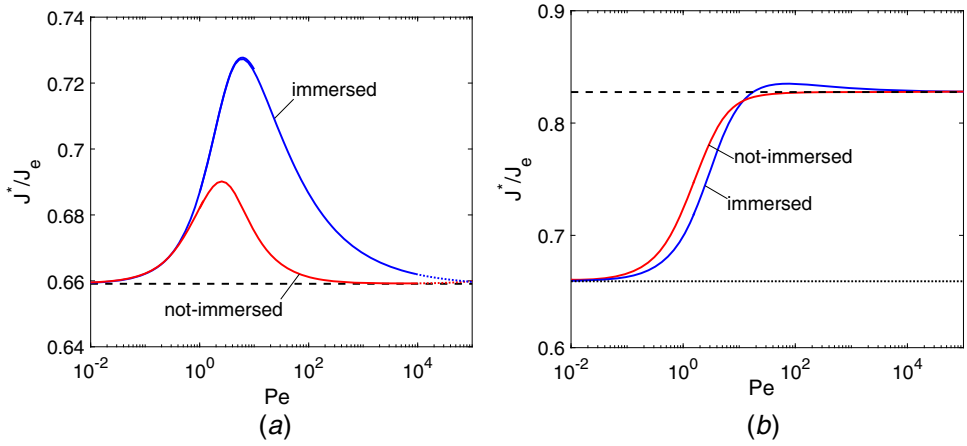


**Fig. 6 Normalized energy release rate ($J^*/J_e$) versus the normalized crack speed ($\mathrm{Pe} = \dot{a}h/D^*$) for steady-state crack growth in linearly poroelastic specimens ($\nu = 0.24$): (*a*) under plane strain conditions and (*b*) under plane stress conditions. The dotted and dashed lines are the slow and fast crack limits, respectively.**

apparent fracture toughness [11,18], which is generally greater than the intrinsic fracture toughness ($J^*/J_e < 1$). Moreover, Eq. (24) implies that the apparent toughness $J_e$ would depend on the specimen size through the Péclet number ($\mathrm{Pe} = \dot{a}h/D^*$) whereas the intrinsic toughness $\Gamma_{ss}$ should be independent of the specimen size.

If the rate-dependent fracture toughness $\Gamma_{ss}(\dot{a})$ is known for the gel, Eq. (24) may be used to predict the steady-state crack speed in a long-strip specimen subject to an applied strain $\varepsilon_\infty$. In particular, if $\Gamma_{ss}$ is independent of the crack speed, there exist two critical strains under the plane strain conditions: $\varepsilon_{c1} = \sqrt{\frac{\Gamma_{ss}}{4Gh\Lambda_{max}}}$ and $\varepsilon_{c2} = \sqrt{\frac{\Gamma_{ss}(1-\nu)}{2Gh}}$, where $\Lambda_{max}$ is the peak value of the function $\Lambda_{ss}(\mathrm{Pe}, \nu)$ as shown in Fig. 6(*a*) for a given Poisson's ratio. If the applied strain is smaller than the first critical strain ($\varepsilon_\infty < \varepsilon_{c1}$), the energy release rate is less than the intrinsic toughness ($J^* < \Gamma_{ss}$) for all crack speeds and thus the crack would not be able to grow at all. Thus, the first critical strain ($\varepsilon_{c1}$) is the threshold strain for steady-state crack growth in the gel. On the other hand, if the applied strain is greater than the second critical strain ($\varepsilon_\infty > \varepsilon_{c2}$), the energy release rate is greater than the intrinsic toughness ($J^* > \Gamma_{ss}$) for all crack speeds and thus no steady-state crack growth is possible without considering inertial effects. Between the two critical strains ($\varepsilon_{c1} < \varepsilon_\infty < \varepsilon_{c2}$), quasi-static steady-state crack growth is possible. Interestingly, the numerical results in Fig. 6(*a*) predict two possible crack speeds under the plane strain conditions, but only one is stable. Considering the change of the energy release rate with a slight perturbation to the crack speed, stable steady-state crack growth is predicted when $\partial\Lambda_{ss}/\partial\mathrm{Pe} < 0$. Therefore, based on Fig. 6(*a*), we plot in Fig. 7 the Péclet number for the stable crack speed versus $J_e/\Gamma_{ss}$ as the normalized loading parameter. Notably, such a plot resembles the V–G curve for environmentally assisted subcritical crack growth in many brittle solids [52], with a threshold energy release rate for slow crack growth and a critical energy release rate for fast fracture.

Experimentally, Baumberger et al. [18] reported measurements of steady-state crack growth in gelatin gels. They found that the applied energy release rate ($J_e$) increased with increasing crack velocity, so-called "velocity toughening," which appears to be consistent with Fig. 7. In addition, they reported that increasing solvent viscosity slowed down the crack growth. By the theory of linear poroelasticity, the solvent viscosity can be related to the effective diffusivity as [42]

$$D^* = \frac{2(1-\nu)}{1-2\nu}\frac{G\kappa}{\eta} \tag{25}$$

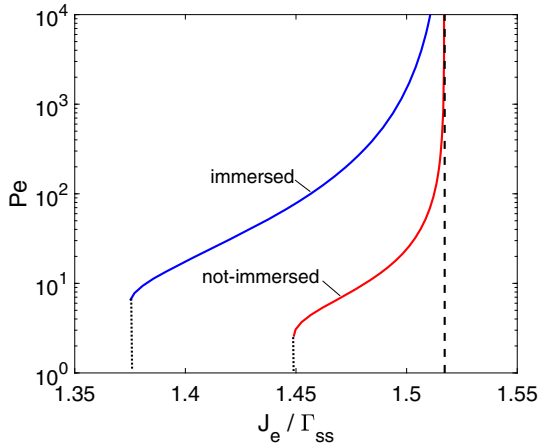


**Fig. 7 Normalized steady-state crack speed ($\mathrm{Pe} = \dot{a}h/D^*$) as a function of the normalized loading parameter ($J_e/\Gamma_{ss}$) for a poroelastic long-strip specimen under plane strain conditions**

where $\eta$ is the solvent viscosity and $\kappa$ is permeability of the polymer network. Thus, increasing the solvent viscosity would decrease the effective diffusivity, which in turn would decrease the crack speed to maintain the same Péclet number ($\mathrm{Pe} = \dot{a}h/D^*$). Furthermore, it was found that soaking the crack tip with the solvent increased the crack velocity. When the applied energy release rate ($J_e$) was too low for the "dry" crack to grow, the "soaked" crack would still grow. The "soaking" effect may be qualitatively understood by comparing the immersed and not-immersed cases in Fig. 7. Under the same applied load ($J_e/\Gamma_{ss}$), the Péclet number for the immersed case ("soaked") is larger than the not-immersed case ("dry") and hence the "soaked" crack grows faster. Moreover, since the threshold load ($\varepsilon_{c1}$ or $J_{e1} = \Gamma_{ss}/\Lambda_{\max}$) for the immersed case is lower than the not-immersed case (assuming same $\Gamma_{ss}$), the "soaked" crack can grow at a lower $J_e$ than the "dry" crack. Therefore, despite the limitations of linear poroelasticity, the numerical results in Fig. 7 are qualitatively consistent with the experiments. Quantitatively, however, the "velocity toughening" observed in the experiments was much more significant than that shown in Fig. 7. Nonlinear poroelasticity and possibly rate-dependent fracture processes should be considered for a more quantitative understanding of the rate-dependent fracture in gels.

Under the plane stress conditions, the numerical results in Fig. 6(*b*) suggest that the crack growth is unstable in the

not-immersed case unless the intrinsic fracture toughness $\Gamma_{ss}$ increases with increasing crack speed. In the immersed case, the normalized energy release rate ($J^*/\Gamma_{ss}$) decreases slightly with increasing crack speed for fast crack growth (Pe > 100), which again is insufficient to account for the "velocity toughening" as observed in experiments [13,18]. To partly account for the rate-dependent fracture processes in gels, a poroelastic cohesive zone model was proposed [25,27], considering both deformation and solvent diffusion in the cohesive zone as follows.

## 5 A Poroelastic Cohesive Zone Model

For the immersed case, a cohesive zone ahead of the crack tip (Fig. 8) is assumed to be permeable to solvent diffusion, where the free energy density (per unit area) is a function of the opening displacement ($\delta$) and the chemical potential ($\mu$) of the solvent [27], namely

$$\phi_c(\delta, \mu) = \frac{1}{2}k\delta^2 - \frac{\mu}{\Omega}\delta \tag{26}$$

with a constant stiffness $k$ and the solvent molecular volume $\Omega$. The opening stress ($\sigma_{22}$) and the solvent concentration ($\zeta$, per unit area) in the cohesive zone can then be obtained as

$$\sigma_{22} = \frac{\partial \phi_c}{\partial \delta} = k\delta - \frac{\mu}{\Omega} \tag{27}$$

$$\zeta = -\frac{\partial \phi_c}{\partial \mu} = \frac{\delta}{\Omega} \tag{28}$$

Equation (27) indicates that the traction-separation relation of the cohesive zone depends on the solvent chemical potential, similar to the pore pressure in linear poroelasticity. By Eq. (28), the opening space in the cohesive zone must be filled up by solvent molecules.

The solvent flux in the cohesive zone is assumed to follow a linear kinetic law [25,27]:

$$j_1 = -M_0 \frac{\partial \mu}{\partial x_1} \tag{29}$$

where the mobility constant $M_0$ is taken to be the same as that in the gel.

Mass conservation in the cohesive zone requires that [27]

$$\frac{\partial \zeta}{\partial t} + \frac{\partial}{\partial x_1}(j_1 \delta) + (j_2^+ - j_2^-) = 0 \tag{30}$$

where $j_2^+$ and $j_2^-$ are the solvent flux rates across the upper and lower interfaces of the cohesive zone at $x_2 = 0^+$ and $x_2 = 0^-$, respectively. The second term in Eq. (30) is nonlinear in general, which was linearized in Ref. [25] by assuming a constant $\delta$.

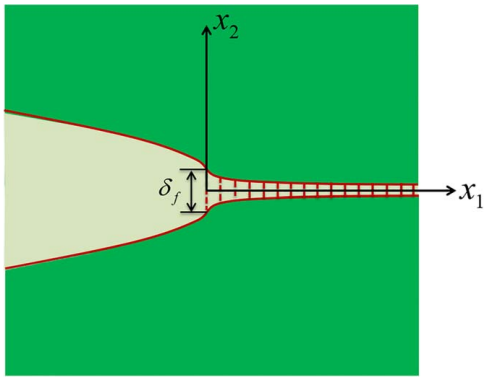


**Fig. 8 Schematic of a cohesive zone model with a crack-tip opening displacement $\delta_f$**

With the poroelastic cohesive zone model, additional energy dissipation occurs due to solvent diffusion within the cohesive zone. The modified $J$-integral in Eq. (3) is path-independent only if the entire cohesive zone is enclosed within the contour. Otherwise, for an arbitrary contour, additional terms must be included in the $J$-integral to account for the energy dissipation within the cohesive zone [27]. By taking an infinitesimal circular contour around the crack tip, we obtain

$$J^* = \left(\frac{1}{2}k\delta^2 - \frac{\mu}{\Omega}\delta\right)\Big|_{x_1=0} \tag{31}$$

For the immersed case, with $\mu = 0$ and $\delta = \delta_f$ at the crack tip ($x_1 = 0$), we obtain $J^* = \frac{1}{2}k\delta_f^2$. Here, $\delta_f$ is the crack-tip opening displacement (CTOD) and, for the case of steady-state crack growth, it is also the critical separation for fracture.

For the not-immersed case, we assume that the cohesive zone is impermeable to solvent diffusion so that the free energy density function (per unit area) is simply $\phi_c = \frac{1}{2}k\delta^2$, and the opening stress is $\sigma_{22} = k\delta$. In this case, we obtain [27]

$$J^* = \frac{1}{2}k\delta_f^2 \tag{32}$$

Note that, while Eq. (32) is the same for both the immersed and not-immersed cases, solvent diffusion in the cohesive zone for the immersed case dissipates energy and thus enhances poroelastic toughening, but the cohesive zone for the not-immersed case is simply elastic with no solvent diffusion.

By dimensional considerations, the normalized energy release rate $J^*/J_e$ for the steady-state crack model (Fig. 5), now with a cohesive zone, depends on four dimensionless parameters, namely

$$\frac{J^*}{J_e} = \Lambda_{ss}\left(\mathrm{Pe}, \varepsilon_\infty, \frac{l_c}{h}, \nu\right) \tag{33}$$

where $l_c = G/k$ is a length scale associated with the cohesive zone. When $l_c/h \to 0$ (no cohesive zone), Eq. (33) reduces to Eq. (21), following the linear poroelastic results. With the cohesive zone, the problem becomes weakly nonlinear as a result of solvent diffusion governed by Eq. (30) for the immersed case.

With the poroelastic cohesive zone model, the stabilized finite element method was modified to account for the traction-separation and solvent diffusion in the cohesive zone [27]. The crack-tip energy release rate can be calculated directly by Eq. (32) for both the immersed and not-immersed cases, where the CTOD ($\delta_f$) depends on the applied strain ($\varepsilon_\infty$) nonlinearly for the immersed case but linearly for the not-immersed case. Figure 9 shows the numerical results for the normalized energy release rate as a function of the Péclet number under the plane stress conditions. Compared with Fig. 6(*b*), the presence of a small-scale cohesive zone ($l_c/h = 10^{-5}$) has no effect on the energy release rate for relatively slow crack growth with Pe < 100. In this case, $l_c \ll l_{ss}$ and the cohesive zone is largely enclosed by the diffusion zone. For fast crack growth (Pe > 100), the diffusion zone size ($l_{ss}$) becomes comparable to or even smaller than the cohesive length scale ($l_c$), and the poroelastic effect is influenced by the cohesive zone. For the immersed case, the normalized energy release rate decreases as the Péclet number increases. For very fast crack growth (Pe > $10^5$), the diffusion length is smaller than the cohesive length ($l_{ss} < l_c \ll h$). In this case, a crack tip model can be used with the elastic K-field imposed as the remote boundary condition [27]. It was found that as $l_c/l_{ss}$ increases, the normalized energy release rate decreases and approaches zero. Apparently, with increasing Péclet number, the magnitude of the chemical potential and its gradient ($\partial\mu/\partial x_1$) in the cohesive zone increase significantly, leading to enhanced energy dissipation within the cohesive zone. Meanwhile, the opening separation in the cohesive zone is proportional to the solvent concentration and thus kinetically constrained by solvent diffusion.

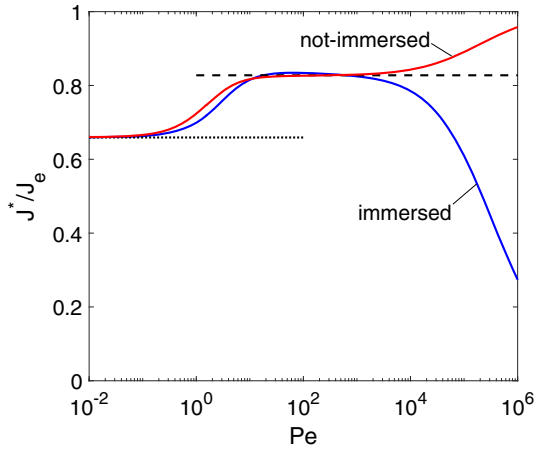


**Fig. 9 Normalized energy release rates versus the Péclet number under the plane stress conditions with the nonlinear cohesive zone model ($\varepsilon_\infty = 10^{-3}$, $l_c/h = 10^{-5}$, and $\nu = 0.24$). The dotted and dashed lines are the slow and fast crack limits without the cohesive zone, respectively.**

For the not-immersed case, with no solvent diffusion in the cohesive zone, the numerical results show the opposite trend for the normalized energy release rate (Fig. 9). Evidently, as the Péclet number increases, the effect of poroelastic toughening decreases in the not-immersed case. Here, solvent diffusion is restricted to a small region near the crack tip, where the presence of a cohesive zone reduces the stress and solvent concentration, leading to reduced energy dissipation by solvent diffusion. In the limiting case of very fast crack growth with $\mathrm{Pe} \gg 1$ or $l_{ss} \ll l_c$, the energy dissipation by solvent diffusion vanishes and the crack-tip energy release rate approaches the elastic limit ($J^*/J_e \to 1$) [27].

With the cohesive zone model, additional measurements are needed to determine the steady-state fracture toughness. For example, the CTOD may be measured as a function of the crack speed, $\delta_f(\dot{a})$. By dimensional considerations, we have

$$\delta_f(\dot{a}) = 2h\varepsilon_\infty \cdot g\left(\mathrm{Pe}, \varepsilon_\infty, \frac{l_c}{h}, \nu\right) \tag{34}$$

where $g\left(\mathrm{Pe}, \varepsilon_\infty, \frac{l_c}{h}, \nu\right)$ is a dimensionless function and can be calculated [27]. Under a given applied strain and crack speed, the crack-tip opening increases with increasing cohesive length ($l_c/h$) so that the cohesive length and the stiffness $k$ can be determined from the measured CTOD. Then, by Eq. (32), the steady-state fracture toughness can be obtained as $\Gamma_{ss}(\dot{a}) = \frac{1}{2}k\delta_f^2$.

With the cohesive zone model, the numerical results in Fig. 9 suggest that the crack growth remains unstable for the not-immersed case unless the steady-state fracture toughness ($\Gamma_{ss}$) increases with increasing crack speed. For the immersed case, significantly enhanced poroelastic toughening is predicted for relatively fast crack growth ($\mathrm{Pe} > 100$). Assuming a constant $\Gamma_{ss}$ (e.g., $\Gamma_{ss} = 10^{-4}Gh$), the applied strain required for the steady-state crack growth at each speed can be determined by setting $J^* = \Gamma_{ss}$ in Eq. (33). Figure 10(*a*) shows the applied energy release rate ($J_e = 4G\varepsilon_\infty^2 h$) thus obtained as a function of the normalized crack speed [27]. Evidently, the effect of poroelastic toughening increases with increasing crack speed ("velocity toughening"). With the poroelastic cohesive zone, the poroelastic toughening is more significant than that shown in Fig. 7 for plane strain conditions without a cohesive zone. Experimentally, Lefranc and Bouchaud [13] found that the measured energy release rate increased significantly with increasing crack speed in agar gels, qualitatively consistent with Fig. 10(*a*), although it may also include effects from other rate-dependent fracture processes at the crack tip.

Further insights were gained by examining the opening displacement, the opening stress, and the chemical potential in the poroelastic cohesive zone at different crack speeds for the immersed case [27], assuming the same fracture toughness ($\Gamma_{ss} = 10^{-4}Gh$). Remarkably, the numerical results suggested a rate-dependent traction-separation relation as shown in Fig. 10(*b*). For relatively slow crack growth ($\mathrm{Pe} = 100$), the chemical potential in the cohesive zone is small and the traction-separation relation is almost linear ($\sigma_{22} \approx k\delta$). As the crack speed increases, the magnitude of chemical potential increases and adds significantly (as a negative pore pressure) onto the opening stress following Eq. (27). As a result, the traction-separation relation becomes nonlinear and dependent on the crack speed. For very fast crack growth ($\mathrm{Pe} = 10^6$), the opening stress reaches a peak ahead of the crack tip where the chemical potential is the most negative. Correspondingly, the traction-separation relation becomes non-monotonic with apparent softening after the peak. With the same steady-state toughness ($\Gamma_{ss} = 10^{-4}Gh$ and $l_c/h = 10^{-5}$), the opening displacement and stress at the crack tip ($x_1 = 0$) are independent of the crack speed, but the trajectory of the traction-separation relation depends on the chemical potential and solvent diffusion within the cohesive zone. Interestingly, by integrating the traction-separation relation we would obtain a rate-dependent fracture energy that includes not only the crack-tip energy release rate ($\Gamma_{ss} = J^*$) but also the energy dissipation in the poroelastic cohesive zone; while the former is assumed to be independent of crack speed here, the latter is inherently rate-dependent. We note that, despite the small-scale bridging condition ($l_c/h = 10^{-5}$), the effect of the poroelastic cohesive zone could be significant when

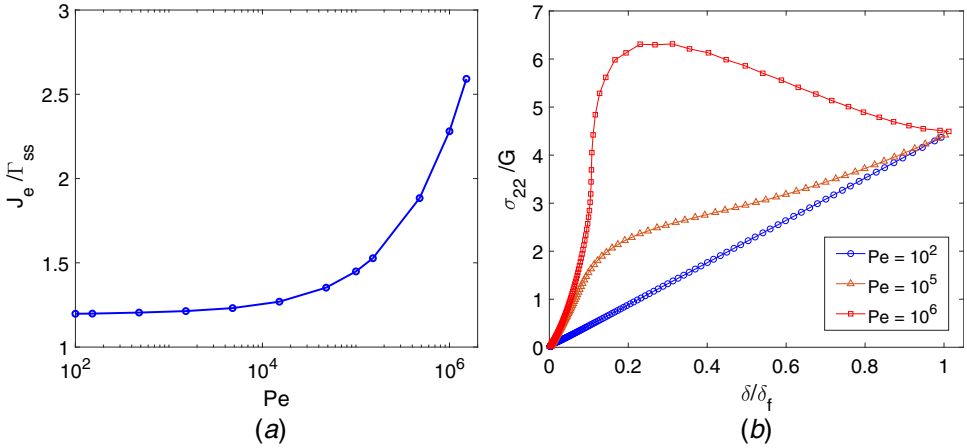


**Fig. 10 (*a*) The applied energy release rate ($J_e = 4G\varepsilon_\infty^2 h$) as a function of the Péclet number for the immersed case under plane stress conditions, with $\Gamma_{ss} = 10^{-4}Gh$, $l_c/h = 10^{-5}$ and $\nu = 0.24$. (*b*) Rate-dependent traction-separation relations by the poroelastic cohesive zone model.**

the diffusion length scale ($l_{ss}/h = 1/\mathrm{Pe}$) is as small as or even smaller than the cohesive length scale as in the case of fast crack growth ($\mathrm{Pe} \gg 1$).

## 6 Closing Remarks

This paper focuses on the effects of poroelasticity on the time- and rate-dependent fracture of polymer gels. A modified $J$-integral is used to calculate the crack-tip energy release rate as the energetic driving force for crack growth in poroelastic gels, taking into account the energy dissipation by solvent diffusion. For a stationary crack, the energy release rate is time-dependent, and delayed fracture can be predicted based on a Griffith-like fracture criterion. For steady-state crack growth in a long-strip specimen, the energy release rate is a function of the crack speed, with rate-dependent poroelastic toughening. With a poroelastic cohesive zone model, solvent diffusion within the cohesive zone leads to significantly enhanced poroelastic toughening as the crack speed increases. While most of the analytical and numerical results are based on the linear poroelastic formulation, future studies may extend to nonlinear theories coupling solvent diffusion with large deformation, especially for tough gels [8,9]. In addition to the poroelastic effects, other mechanisms such as viscoelasticity and local fracture processes should be studied to further understand the time- and rate-dependent fracture of polymer gels. Of particular interest is the phase-field modeling [53,54] that may incorporate various deformation and fracture mechanisms within a unified theoretical and computational framework.


## Funding Data

- National Science Foundation (Grant No. CMMI-1538658; Funder ID: 10.13039/501100008982).


## References


[1] Drury, J. L., and Mooney, D. J., 2003, "Hydrogels for Tissue Engineering: Scaffold Design Variables and Applications," Biomaterials, **24**(24), pp. 4337–4351.
[2] Langer, R., 2006, "Biomaterials for Drug Delivery and Tissue Engineering," MRS Bull., **31**(6), pp. 477–485.
[3] Peppas, N. A., Hilt, J. Z., Khademhosseini, A., and Langer, R., 2006, "Hydrogels in Biology and Medicine: From Molecular Principles to Bionanotechnology," Adv. Mater., **18**(11), pp. 1345–1360.
[4] Calvert, P., 2009, "Hydrogels for Soft Machines," Adv. Mater., **21**(7), pp. 743–756.
[5] Suo, Z., 2012, "Mechanics of Stretchable Electronics and Soft Machines," MRS Bull., **37**(3), pp. 218–225.
[6] Yuk, H., Lin, S. T., Ma, C., Takaffoli, M., Fang, N. X., and Zhao, X., 2017, "Hydraulic Hydrogel Actuators and Robots Optically and Sonically Camouflaged in Water," Nat. Commun., **8**, p. 14230.
[7] Yang, C., and Suo, Z., 2018, "Hydrogel Ionotronics," Nat. Rev. Mater., **3**, pp. 125–142.
[8] Gong, J. P., Katsuyama, Y., Kurokawa, T., and Osada, Y., 2003, "Double-Network Hydrogels With Extremely High Mechanical Strength," Adv. Mater., **15**(14), pp. 1155–1158.
[9] Sun, J. Y., Zhao, X. H., Illeperuma, W. R. K., Chaudhuri, O., Oh, K. H., Mooney, D. J., Vlassak, J. J., and Suo, Z., 2012, "Highly Stretchable and Tough Hydrogels," Nature, **489**(7414), pp. 133–136.
[10] Zhao, X., 2014, "Multi-scale Multi-Mechanism Design of Tough Hydrogels: Building Dissipation Into Stretchy Networks," Soft Matter, **10**(5), pp. 672–687.
[11] Long, R., and Hui, C. Y., 2016, "Fracture Toughness of Hydrogels: Measurement and Interpretation," Soft Matter, **12**(39), pp. 8069–8086.
[12] Creton, C., 2017, "50th Anniversary Perspective: Networks and Gels: Soft but Dynamic and Tough," Macromolecules, **50**(21), pp. 8297–8316.
[13] Lefranc, M., and Bouchaud, E., 2014, "Mode I Fracture of a Biopolymer gel: Rate-Dependent Dissipation and Large Deformations Disentangled," Extreme Mech. Lett., **1**, pp. 97–103.
[14] Forte, A. E., D'Amico, F., Charalambides, M. N., Dini, D., and Williams, J. G., 2015, "Modelling and Experimental Characterisation of the Rate Dependent Fracture Properties of Gelatine Gels," Food Hydrocolloid, **46**, pp. 180–190.
[15] Bonn, D., Kellay, H., Prochnow, M., Ben-Djemiaa, K., and Meunier, J., 1998, "Delayed Fracture of an Inhomogeneous Soft Solid," Science, **280**(5361), pp. 265–267.
[16] Skrzeszewska, P. J., Sprakel, J., de Wolf, F. A., Fokkink, R., Stuart, M. A. C., and van der Gucht, J., 2010, "Fracture and Self-Healing in a Well-Defined Self-Assembled Polymer Network," Macromolecules, **43**(7), pp. 3542–3548.
[17] Tang, J., Li, J., Vlassak, J. J., and Suo, Z., 2017, "Fatigue Fracture of Hydrogels," Extreme Mech. Lett., **10**, pp. 24–31.
[18] Baumberger, T., Caroli, C., and Martina, D., 2006, "Solvent Control of Crack Dynamics in a Reversible Hydrogel," Nat Mater, **5**(7), pp. 552–555.
[19] Wang, X., and Hong, W., 2012, "Delayed Fracture in Gels," Soft Matter, **8**(31), pp. 8171–8178.
[20] Bouklas, N., Landis, C. M., and Huang, R., 2015, "Effect of Solvent Diffusion on Crack-Tip Fields and Driving Force for Fracture of Hydrogels," ASME J. Appl. Mech., **82**(8), p. 081007.
[21] Atkinson, C., and Craster, R. V., 1991, "Plane Strain Fracture in Poroelastic Media," Proc. R. Soc. London, A, **434**(1892), pp. 605–633.
[22] Hui, C. Y., Long, R., and Ning, J., 2013, "Stress Relaxation Near the Tip of a Stationary Mode I Crack in a Poroelastic Solid," ASME J. Appl. Mech., **80**(2), p. 021014.
[23] Yang, C.-H., and Lin, Y.-Y., 2018, "Time-Dependent Fracture of Mode-I Cracks in Poroviscoelastic Media," Eur. J. Mechanics—A/Solids, **69**, pp. 78–87.
[24] Yu, Y., Bouklas, N., Landis, C. M., and Huang, R., 2018, "A Linear Poroelastic Analysis of Time-Dependent Crack-Tip Fields in Polymer Gels," ASME J. Appl. Mech., **85**(11), p. 111011.
[25] Noselli, G., Lucantonio, A., McMeeking, R. M., and DeSimone, A., 2016, "Poroelastic Toughening in Polymer Gels: A Theoretical and Numerical Study," J. Mech. Phys. Solids, **94**, pp. 33–46.
[26] Yu, Y., Landis, C. M., and Huang, R., 2018, "Steady-State Crack Growth in Polymer Gels: A Linear Poroelastic Analysis," J. Mech. Phys. Solids, **118**, pp. 15–39.
[27] Yu, Y., Landis, C. M., and Huang, R., 2019, "Poroelastic Effects on Steady State Crack Growth in Polymer Gels Under Plane Stress," Mech. Mater. (submitted).
[28] Rice, J. R., 1968, "A Path Independent Integral and the Approximate Analysis of Strain Concentration by Notches and Cracks," ASME J. Appl. Mech., **35**(2), pp. 379–386.
[29] Yang, C., Yin, T., and Suo, Z., 2019, "Polyacrylamide Hydrogels. I. Network Imperfection," J. Mech. Phys. Solids, **131**, pp. 43–55.
[30] Irwin, G., 1948, *Fracturing of Metals*, ASM, Cleveland, p. 147.
[31] Orowan, E., 1950, "Fatigue and Fracture of Metals," Symposium at Massachusetts Institute of Technology, New York.
[32] Knauss, W. G., 1970, "Delayed Failure—the Griffith Problem for Linearly Viscoelastic Materials," Int. J. Fracture Mechanics, **6**(1), pp. 7–20.
[33] Knauss, W. G., 1973, "The Mechanics of Polymer Fracture," ASME Appl. Mech. Rev., **26**(1), pp. 1–17.
[34] Schapery, R. A., 1975, "A Theory of Crack Initiation and Growth in Viscoelastic Media," Int. J. Fract., **11**(1), pp. 141–159.
[35] Schapery, R. A., 1975, "A Theory of Crack Initiation and Growth in Viscoelastic Media II. Approximate Methods of Analysis," Int. J. Fract., **11**(3), pp. 369–388.
[36] Schapery, R. A., 1975, "A Theory of Crack Initiation and Growth in Viscoelastic Media," Int. J. Fract., **11**(4), pp. 549–562.
[37] Schapery, R. A., 1984, "Correspondence Principles and a Generalized J Integral for Large Deformation and Fracture Analysis of Viscoelastic Media," Int. J. Fract., **25**(3), pp. 195–223.
[38] Bouklas, N., Landis, C. M., and Huang, R., 2015, "A Nonlinear, Transient Finite Element Method for Coupled Solvent Diffusion and Large Deformation of Hydrogels," J. Mech. Phys. Solids, **79**, pp. 21–43.
[39] Kishimoto, K., Aoki, S., and Sakata, M., 1980, "On the Path Independent Integral-J," Eng. Fract. Mech., **13**(4), pp. 841–850.
[40] Yang, F., Wang, J., and Chen, D., 2006, "The Energy Release Rate for Hygrothermal Coupling Elastic Materials," Acta Mech. Sin., **22**(1), pp. 28–33.
[41] Gao, Y. F., and Zhou, M., 2013, "Coupled Mechano-Diffusional Driving Forces for Fracture in Electrode Materials," J. Power Sources, **230**, pp. 176–193.
[42] Bouklas, N., and Huang, R., 2012, "Swelling Kinetics of Polymer Gels: Comparison of Linear and Nonlinear Theories," Soft Matter, **8**(31), pp. 8194–8203.
[43] Biot, M. A., 1941, "General Theory of Three-Dimensional Consolidation," J. Appl. Phys., **12**(2), pp. 155–164.
[44] Petch, N. J., and Stables, P., 1952, "Delayed Fracture of Metals Under Static Load," Nature, **169**, pp. 842–843.
[45] Pearson, S., 1956, "Delayed Fracture of Sintered Alumina," P. Phys. Soc. B, **69**(12), pp. 1293–1296.
[46] Lindstrom, S. B., Kodger, T. E., Sprakel, J., and Weitz, D. A., 2012, "Structures, Stresses, and Fluctuations in the Delayed Failure of Colloidal Gels," Soft Matter, **8**(13), pp. 3657–3664.
[47] Shahidzadeh-Bonn, N., Vie, P., Chateau, X., Roux, J.-N., and Bonn, D., 2015, "Delayed Fracture in Porous Media," Phys. Rev. Lett., **95**(17), pp. 175501.
[48] van der Kooij, H. M., Dussi, S., van de Kerkhof, G. T., Frijns, R. A. M., van der Gucht, J., and Sprakel, J., 2018, "Laser Speckle Strain Imaging Reveals the Origin of Delayed Fracture in a Soft Solid," Sci. Adv., **4**(5), p. eaar1926.
[49] Rivlin, R. S., and Thomas, A. G., 1953, "Rupture of Rubber. I. Characteristic Energy for Tearing," J. Poly. Sci., **10**(3), pp. 291–318.
[50] Franca, L. P., Frey, S. L., and Hughes, T. J. R., 1992, "Stabilized Finite-Element Methods 1. Application to the Advective-Diffusive Model," Comput. Meth. Appl. Mech. Eng., **95**(2), pp. 253–276.
[51] Hutchinson, J. W., 1983, "Fundamentals of the Phenomenological Theory of Nonlinear Fracture Mechanics," ASME J. Appl. Mech., **50**(4b), pp. 1042–1051.
[52] Lawn, B., 1993, *Fracture of Brittle Solids*, 2nd ed., Cambridge University Press, Cambridge, UK.
[53] Böger, L., Keip, M.-A., and Miehe, C., 2017, "Minimization and Saddle-Point Principles for the Phase-Field Modeling of Fracture in Hydrogels," Comput. Mater. Sci., **138**, pp. 474–485.
[54] Mao, Y., and Anand, L., 2018, "A Theory for Fracture of Polymeric Gels," J. Mech. Phys. Solids, **115**, pp. 30–53.